FREE-SURFACE MULTIPLE PREDICTION AND SUBTRACTION FROM SLOWNESS RELATIONS IN 2D AND 3D SYNTHETIC DATA

JUANJUAN CAO and GEORGE A. MCMECHAN

Center for Lithospheric Studies, The University of Texas at Dallas, 800 W Campbell Road, Richardson, TX 75080-3021, U.S.A.

(Received May 17, 2011; revised version accepted June 7, 2011)

ABSTRACT

Cao, J. and McMechan, G.A., 2011. Free-surface multiple prediction and subtraction from slowness relations in 2D and 3D synthetic data. *Journal of Seismic Exploration*, 20: 235-255.

A target-oriented, data-adaptive, algorithm is developed for the prediction and subtraction of free-surface multiples from seismic data, without knowledge of the subsurface velocities. It uses only slowness relations between the primary reflections on split-spread common-source and common-receiver gathers. It is based on matching slownesses at all source and receiver locations and combining offsets and times of primary reflections to kinematically predict multiples. Our use of only the slownesses p in the multiple prediction eliminates many of the assumptions and complexities that are involved in previous algorithms. This method is extended to 3D and to predict all higher-order multiples. The inputs are the traveltimes, of the primary reflections that produce the multiples, picked from common-source gathers. The subtraction involves flattening the multiple events on their predicted traveltime trajectories, estimating and subtracting a local spatial average trace from the center trace in a moving trace window, and then shifting each trace back to its original time. The effectiveness of this algorithm is illustrated using 2D and 3D synthetic examples. Multiple reduction is clearly visible in common-source and common-offset sections, before and after prestack migration.

KEY WORDS: multiple subtraction, 3D, slowness.

0963-0651/11/$5.00

INTRODUCTION

Multiple attenuation is a challenge in seismic imaging and reservoir characterization. Multiple reflections can be surface-related or internal, depending on the location of the interfaces causing downward propagating reflections. Surface-Related Multiple Elimination (SRME) (Verschuur, 1991; Verschuur and Berkhout, 1992; Verschuur and Berkhout, 1997; Van Dedem, 2002) is the industry standard for surface multiple elimination. It uses the data to predict first-order multiples by convolving the data with itself; it is a data-driven method; the main advantage is that no subsurface information is needed as it is implicitly included within the seismic data. Three-dimensional (3D) SRME (Biersteker, 2001; Van Dedem, 2002; Van Dedem and Verschuur, 2005) assumes that the data are densely sampled on regular grids of sources and receivers. Although data reconstruction (regularization, interpolation and extrapolation), are required to generate ideal datasets to ensure successful predictions, 3D SRME has become commercially available.

Berkhout (1982) developed a feedback model for free-surface multiple generation and attenuation. Inverse scattering multiple attenuation (Gasparotto et al.,1994; Weglein et al., 1997; Kelamis et al., 2006; Berkhout and Verschuur, 2007a,b) removes free-surface and internal multiples of first and higher orders from seismic data without any knowledge of the subsurface. Berkhout (2006) uses an inversion data space approach.

After prediction of surface-related multiples, they are usually subtracted using a least squares matched filter technique (Verschuur and Berkhout, 1997); other adaptive subtraction methods, such as expanded multichannel matched filtering (Huo and Wang, 2009) and curvelet-domain multiple-primary separation (Herrmann et al., 2008), are also available.

There is a group of multiple prediction algorithms that are based on combining attributes of primary reflections to predict multiples; the algorithm that we describe below is in this group, but it has a number of specific advantages over the previous implementations. Landa et al. (1999a) and Zaske (2000) combine primary reflections to form multiples by calculating emergence angles to define ray paths of multiples that are removed in the τ-p domain. Keydar et al. (1998) and Landa et al. (1999b) use both angles and radii of wavefront curvature. Surface multiples and primaries can be separated and subtracted by muting in the inverse coupled plane-wave domain (Ma et al., 2009). Liu et al. (2000) use coupling of slownesses to predict multiples with the knowledge of reflector dips and the source wavelet. Landa et al. (1999b) use emergence angles and radii of wavefront curvature to construct multiples (including internal multiples) by adding and subtracting specific primary reflections. Reshef et al. (2006) also combine primary reflections to predict multiples, using Fermat's principle for zero-offset times, in the time domain,

and include prediction of internal multiples. Below, we develop a similar, data-driven, target-oriented 3D algorithm using only apparent slownesses to predict kinematic properties of free-surface multiples in split-spread common-source gathers without needing any information on subsurface velocities, so multiples can be subtracted even when velocity information is not available. It is target-oriented in the sense that the multiples to be predicted can be individually specified. Our use of only the slownesses p eliminates many of the assumptions and complexities that are involved in these previous algorithms; we do not need incident angles, velocities, radii of curvature, propagation paths, or the geometries of the free surface or of the reflectors. Unlike SRME, it does not do any wavefield convolutions, and so it is very cost effective.

Applications, of p-based multiple removal, to 2D synthetic and field ocean-bottom cable data are previously presented by Cao and McMechan (2010). Here, this method is adapted for 3D data acquired using surface sources and receivers, and we attenuate free-surface multiples of first-and higher-orders, and some internal multiples. Both 2D and 3D synthetic examples illustrate the procedures for prediction and subtraction. Evaluation of the results in common-offset gathers and before and after prestack migration shows the improvement of subsurface images after multiple attenuation.

ALGORITHM

Prediction of free-surface multiples with a 2D example

Fig. 1 shows free-surface multiple reflections recorded for a survey containing sources(S_1, S_2, S_3, ...), and receivers (R_1, R_2, R_3, ...). Consider two primary reflections, arriving at receiver R_1 from the same reflector, from two sources, S_1 and S_2, with apparent slownesses of the same value but of opposite sign ($+p_1$ and $-p_1$). Because the incident and reflection angles are equal at R_1, the apparent horizontal phase velocities of the incident and reflected waves are equal. As a consequence of source-receiver reciprocity, the first-order multiple can be thought of as combining these two primary paths which are connected to each other at the surface reflection point R_1. Similarly, the second-order multiple from source S_1 has an additional reflection at S_2 and is recorded at R_2; its path consists of segments S_1-R_1-S_2-R_2. The opposite signs of the apparent slownesses at all reflection points are used to define the times and offsets of complete paths corresponding to multiples, by matching apparent slownesses at each S and R point along the path in turn; the actual paths are not needed and are not constructed. When matching apparent slownesses at any single point, the velocity and reflector shape (or free surface topography if it's land data) are common to both path segments and so do not have to be known. By combining primary reflections that are already available in the data, primaries produce multiples and multiples produce higher-order multiples. As

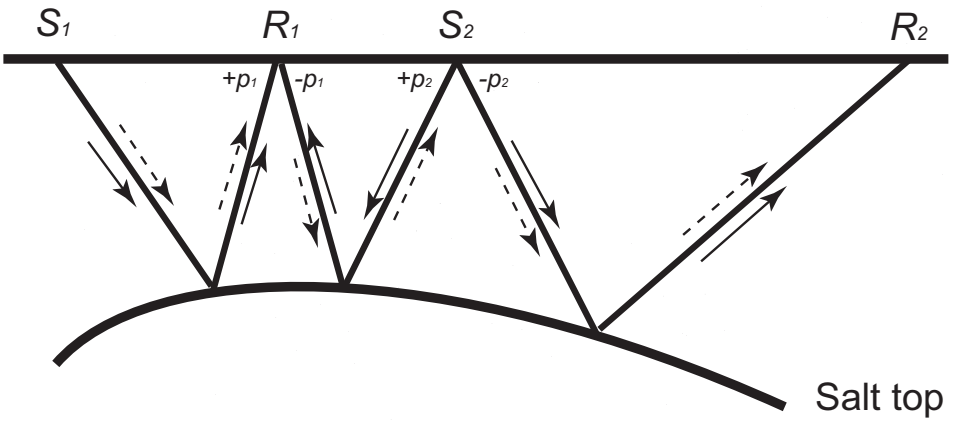

Fig. 1. A raypath associated with free-surface multiples. Solid arrows indicate propagation directions for the primary reflections; dashed arrows indicate those for the first- and second-order multiples from source S_1.

apparent slownesses are matched along the free surface, the surface topography does not have to be flat.

Traveltimes and offsets, of each of the primary S-R combinations, are extracted from the reflected waves in common-source data. Then, the traveltimes and offsets of the multiples can be predicted by combining the traveltime and offset contributions from all the primary S-R segments included in the multiple path, without needing the actual propagation paths or the velocities through which they travel. Although p-values for both common-source and common-receiver gathers (CSGs and CRGs) are needed to correctly identify and concatenate primary reflection segments to predict their multiples, this does not require sorting the data into common-receiver gathers; re-ordering the time picks from the CSGs allows calculating p-values corresponding to the CRGs, and so is computationally efficient. By concatenating times and offsets of the primary paths (by matching opposite-signed slownesses at S and R points alternately in the p-value distributions for CSGs and CRGs), higher-order multiples can also be predicted. Only the first- and second-order multiples are predicted in this paper to demonstrate the algorithm.

Fig. 2 illustrates the trajectories between p-values (computed for CSGs and CRGs to predict multiples from the times picked in the CSGs) by the selection of S-R combinations by matching measured slowness values alternately in CSGs and CRGs (to satisfy Snell's law). In Fig. 2, the slowness $+p_1$ is measured at receiver R_1 in CSG S_1, and then a search is performed to find S_2 which has slowness $-p_1$ at R_1. The combinations of the measured traveltimes and offsets of these two primary reflections define the traveltime and offset of the first multiple ($S_1 R_1 S_2$ in Fig. 1). Similarly, R_2 can be found by measuring

slowness $+p_2$ at source S_2 in CRG R_1 and finding the trace with $-p_2$ at S_2 in CRG R_2. Adding the traveltime and offset contributions of these three primary reflections, completes the whole path S_1-R_1-S_2-R_2 associated with the second multiple (Fig. 2). The paths themselves are not defined, but the times and offsets at the surface are; the latter are sufficient to predict and subtract the multiples, as illustrated in the examples below. Details are presented by Cao and McMechan (2010).

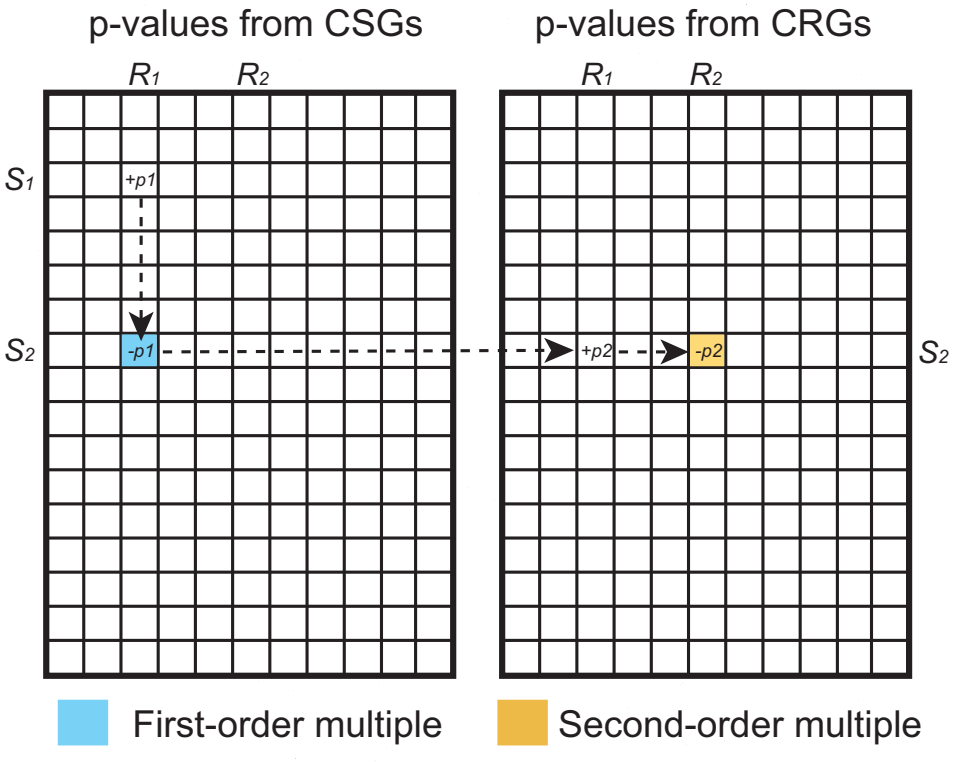

Fig. 2. Trajectory for calculation of the first and second multiples in Fig. 1 by matching slownesses of reflected waves in CSGs and CRGs in 2D data.

Prediction of free-surface multiples in 3D

Consider Fig. 1 in the context of a 3D raypath in a 3D survey containing surface sources and receivers. At each S and R point in 3D, there are reflected waves emitted toward, or arriving from, various 3D CSGs and CRGs around the reflection points. As the reflections in 3D data are surfaces rather than lines (Fig. 3), the apparent horizontal slowness p at each point on the primary reflections is a vector which has two perpendicular horizontal components, p_x and p_y, in the inline and crossline directions, respectively (Fig. 3). Thus, at

receiver R_1, we calculate the apparent horizontal slowness vector components (say $+p_{1x}$ and $+p_{1y}$), then we search R_1 to find S_2 which has slowness components ($-p_{1x}$ and $-p_{1y}$) at R_1. The traveltime and offset of the first multiple S_1-R_1-S_2 are obtained by combining traveltimes and offsets of segments S_1-R_1 and R_1-S_2 which are individually recorded as the primary reflections in the CSGs S_1 and S_2 and CRG R_1 (Fig. 3). Similarly, the second multiple is predicted by finding receiver gather R_2 which has $-p_{2x}$ and $-p_{2y}$ at reflection point S_2 where receiver gather R_1 has $+p_{2x}$ and $+p_{2y}$. The signs of the p components depend on the azimuthal quadrant, the propagation paths, and the reflector dips. Thus, in general, $+p_{ix}$ and $+p_{iy}$ may or may not have the same signs.

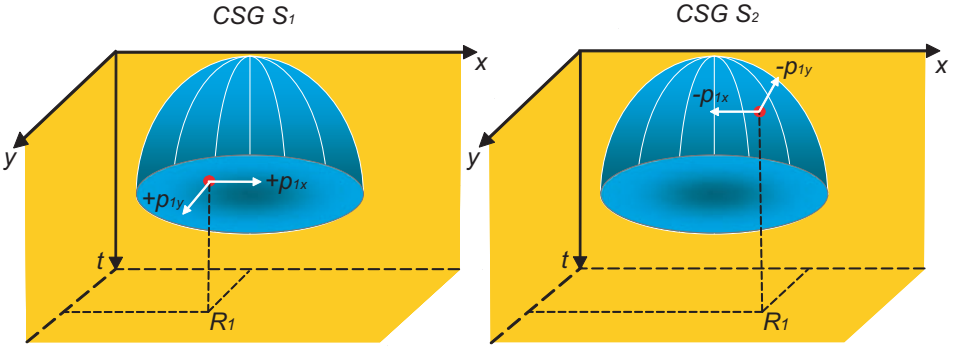

Fig. 3. Two horizontal components p_x and p_y of the slowness vector.

Fig. 4 demonstrates the trajectories between the p-values corresponding to the CSGs and CRGs needed to predict multiples by matching both measured x and y apparent horizontal slowness components at S and R reflection points alternately. Multiples are predicted from the primary reflections that already exist in the seismic data (without any subsurface knowledge, as this information is implicitly contained in the calculated apparent slownesses). The multiples to be predicted (and hence subtracted) need to be specified, by choosing the corrresponding combination of primaries, so the process is inherently target-oriented.

SUBTRACTION OF MULTIPLES

Subtraction of a multiple involves estimation of a local wavelet in the time-space domain. There are three steps: (1) flattening the multiple event by shifting the predicted time of the multiple on each trace to the same reference

time; (2) calculating a local spatial average trace, within a time window, and subtracting this from the center trace in the trace window; and (3) shifting each trace back to its original time (Cao and McMechan, 2010). The primary and multiple reflections are lines in 2D data, and are surfaces in 3D. After flattening for one multiple, that multiple becomes a horizontal line in 2D and a horizontal plane in 3D, and the other (primary and multiple) reflections are curved as they have different move-outs. The local spatial average traces are calculated in a trace window which is centered at the trace under consideration; this window is shifted horizontally in both x and y, to center on each trace in turn. In 2D, the trace window includes a specified number of traces in the offset direction; in 3D, it becomes a small volume window which includes a specified number of inline and crossline traces, with the trace located at the center of the plane.

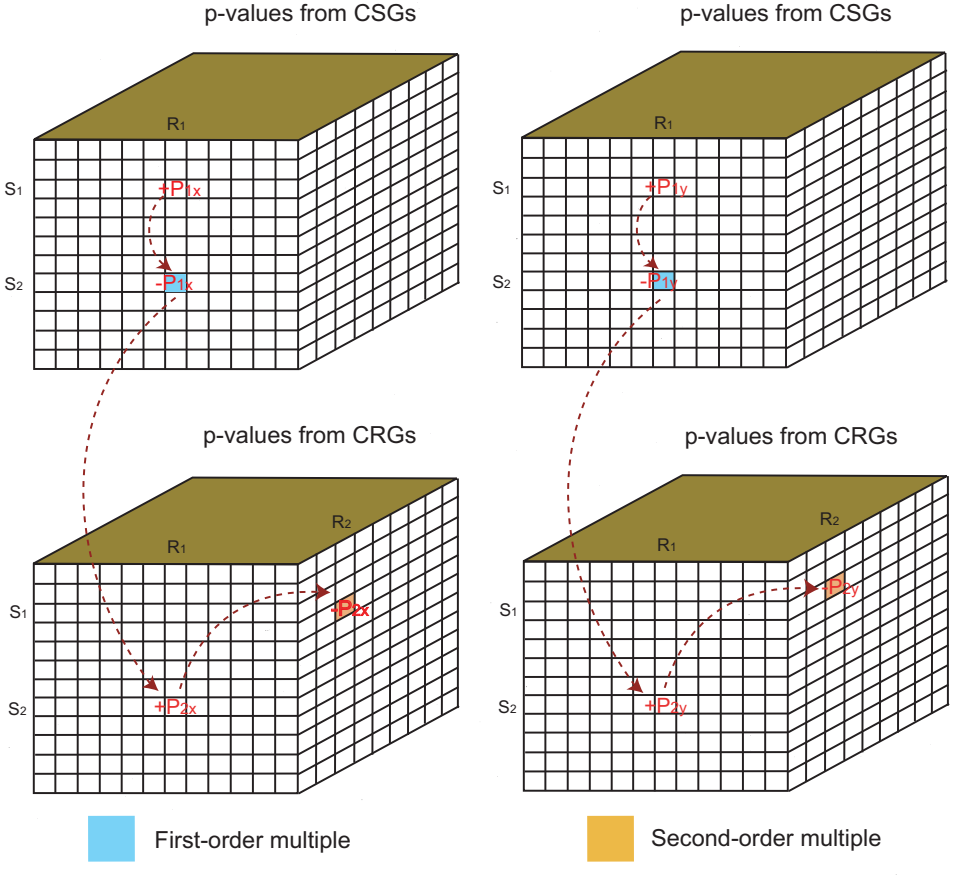

Fig. 4. Trajectory for calculation of the first multiples (upper volumes), and second multiples (lower volumes), in Fig. 1 by matching slownesses on reflected waves in CSGs and CRGs of 3D data. The two left volumes contain the x-component of p; the two right volumes contain the y-component of p. Vertical axes are source positions (CSGs); horizontal axes are inline and crossline receiver positions (two component CRGs).

The subtraction implicitly includes amplitude and phase information when the local average trace is calculated in the time window that contains the multiple (Cao and McMechan, 2010). Internal multiples which lie parallel to the low order multiples from the large primaries, are implicitly removed in the same subtraction as for a primary, by increasing the time window of the subtraction; see Fig. 12 of Cao and McMechan (2010) for a 2D field data example. The procedure of Landa et al. (1999b) can also subtract internal multiples, but uses explicit prediction of each, which is costly compared to our p-based approach. Calculating the local average wavelet in each trace window makes the subtraction data adaptive with respect to wavelet shape and amplitude along the time-space trajectory of the multiple. Details are elaborated, with 2D examples, by Cao and McMechan (2010).

There needs to be differences between the p-values of the primaries and the multiples for the subtraction to work. This is also affected by the width (in offset) of the window within which the averaging subtraction is done; a wider trace window is needed if the primary and multiple reflections are similar.

TESTS ON SYNTHETIC 2D AND 3D DATA

The proposed algorithm is tested by applying it to synthetic data generated from a modified version (http://research.seg.org/3dmodel/salthome/intro.html) of the 2D SEG/EAEG salt model and from a 3D velocity model containing a dipping water layer and sedimentary structures.

2D example

The first dataset is simulated from the 2D SEG/EAEG salt model, to which a dipping water bottom is added (Fig. 5a); this model contains a high-velocity salt body embedded in a low velocity sedimentary background. The model has grid dimensions 2338 $\times$ 417 with grid increments of 10 meters. Here, 67 synthetic scalar split-spread CSGs are generated by finite differencing. Free-surface and absorbing boundary conditions are used at the top, and at the three other edges of the model, respectively. Each CSG has 1000 channels; the source and receiver spacings are 200 m and 10 m, respectively. After interpolation of times, the effective number of CSGs becomes 1321. Each trace has 7500 samples and is 7.5 seconds in duration. The traveltimes of the primary reflections from the salt top, as picked from the CSGs, are displayed in Fig. 5b. Fig. 6 shows p-values of the corresponding primary reflections in the CSGs, and in the corresponding CRGs. The p-values are not symmetric because the reflectors are dipping.

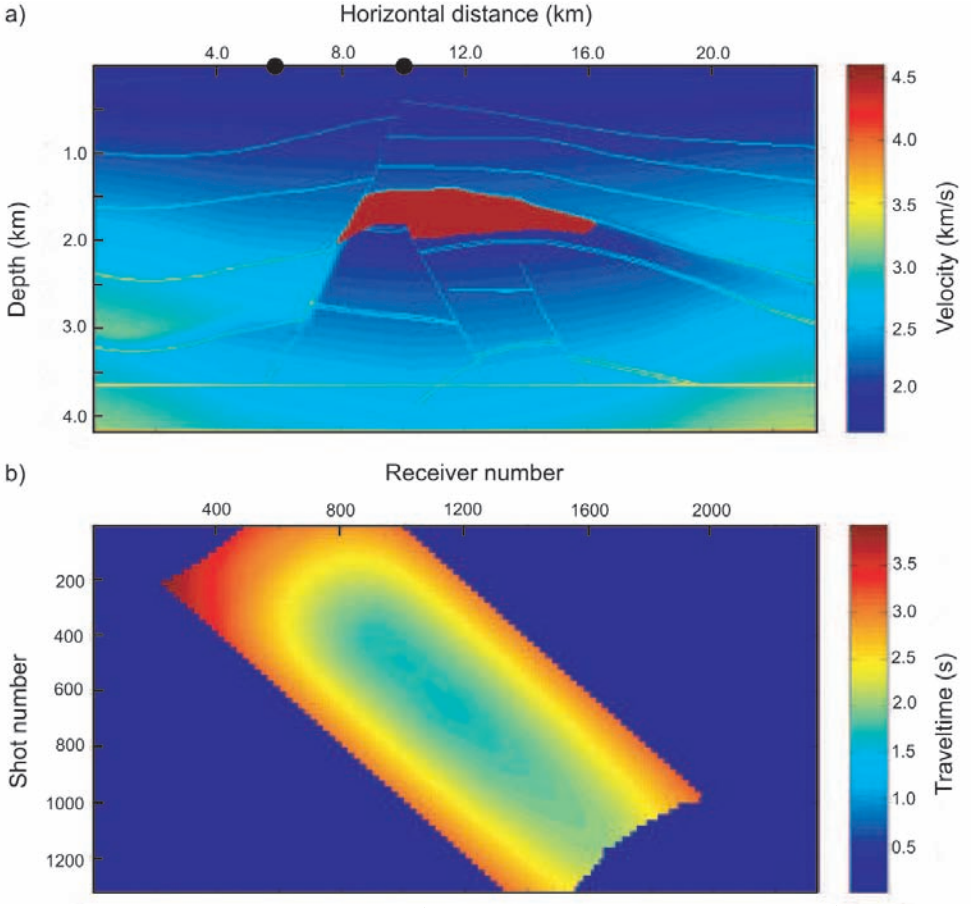

Fig. 5. Velocity model and traveltimes. (a) Contains a 2D cross section of the SEG salt model used to generate synthetic CSGs for free-surface multiple prediction and subtraction. The increments of sources and receivers are 200 m and 10 m, respectively. (b) Contains the interpolated traveltimes of the split-spread primary reflections from the salt top, picked from the CSGs. In (a), the dots at 5.8 km and 10.0 km at the top of the model are the locations of the sources for the two representative CSGs in Fig. 7.

In the two representative CSGs in Fig. 7, the superimposed green curves are the predictions of the first-, second- and third-order multiples (Fig. 7b). They fit the actual multiples in the data very well. Fig. 7c are the same two CSGs after multiple removal. As expected, the free-surface multiples are significantly reduced.

To examine the performance of the proposed algorithm, 2D prestack Kirchhoff depth migration is done for all 67 CSGs, without and with multiple removal. The migration velocity model used is a smoothed version of the SEG salt model in Fig. 5a. One migrated CSG (Fig. 8) demonstrates the effectiveness

of the multiple subtraction. After subtraction of the multiples from the input CSGs, a good subsurface image is obtained by prestack migration of the whole line (Fig. 9). Reflections that were obscured beneath the high amplitude multiples in the migration of the data with multiples (Fig. 9b) are now visible; compare at the arrows in Figs. 9a and c.

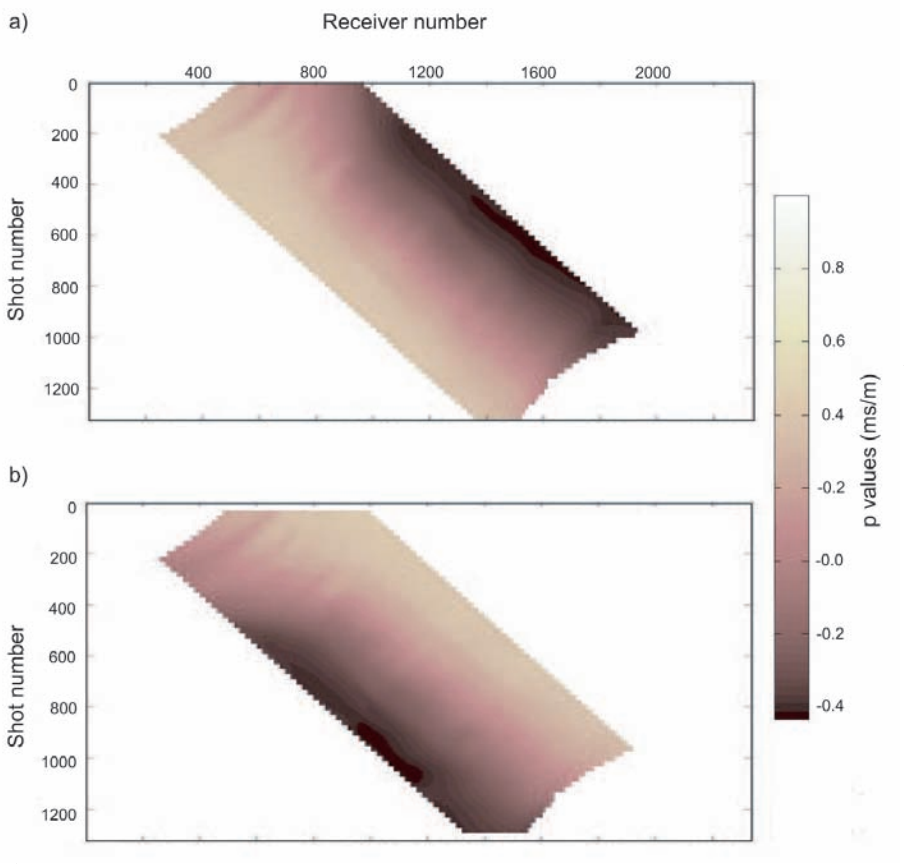

Fig. 6. (a) p-values of the primary reflected waves from the salt top in CSGs. (b) p-values of the primary reflected waves from the salt top in CRGs. Shot numbers are after interpolation of the times.

3D example

In this section, the effectiveness of the proposed method is demonstrated by applying it to a 3D synthetic scalar dataset which was generated from a model (Fig. 10) by finite differencing. The model contains water with a dipping bottom reflector overlying sedimentary structures. The model has grid dimensions 390 × 390 × 160 with grid increment 5 meters. There are 484

CSGs (a 22 × 22 source array); each CSG contains traces in a 167 × 167 (inline × crossline) array of receivers that cover the top surface of the model. The sources are separated by 50 m in both the inline and crossline directions; the receivers are separated by 5 meters. The recording sampling increment is 0.5 ms; the total recording time is 1 s. Free-surface and absorbing boundary conditions are used at the top, and at the other five bounding planes of the model, respectively.

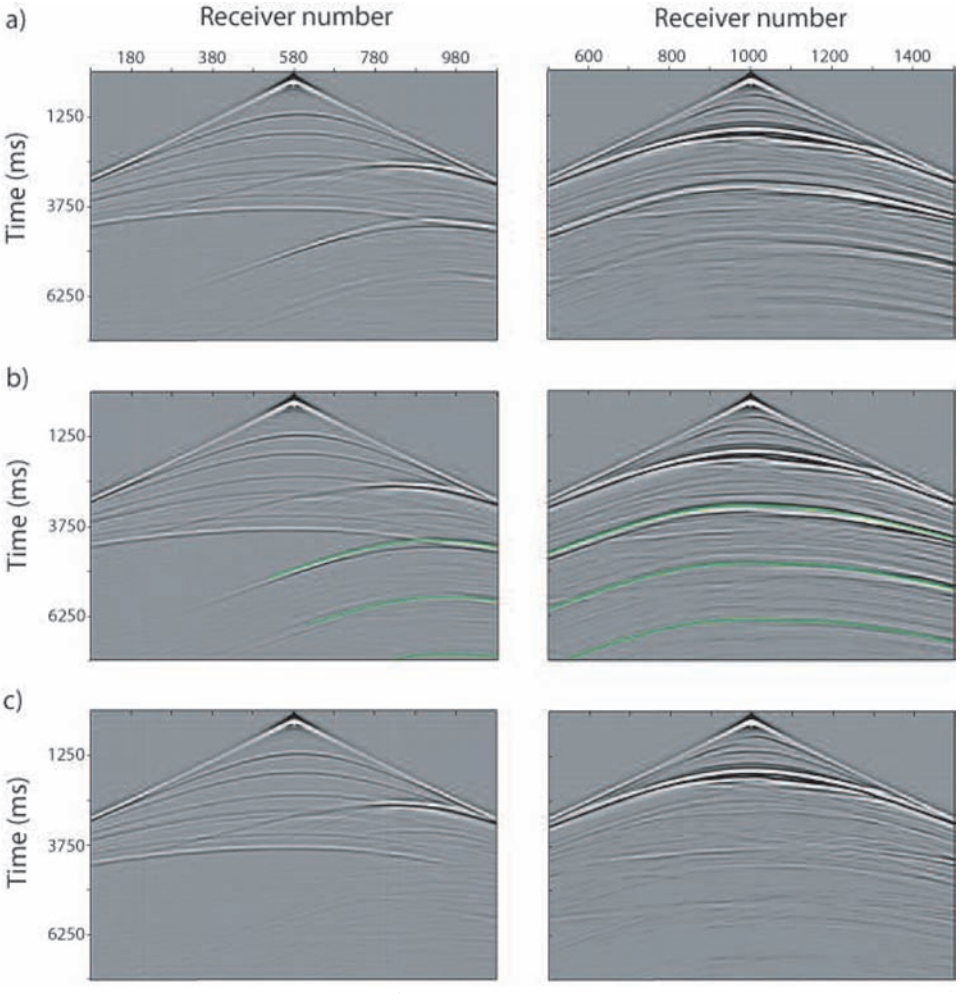

Fig. 7. Two representative input CSGs (a) for the model in Fig. 5a with (the green line) predictions of free-surface multiples (b) before, and (c) after, multiple removal. The trace increment is 10 m. The locations of these two sources are the black dots shown at the surface of the model in Fig. 5a.

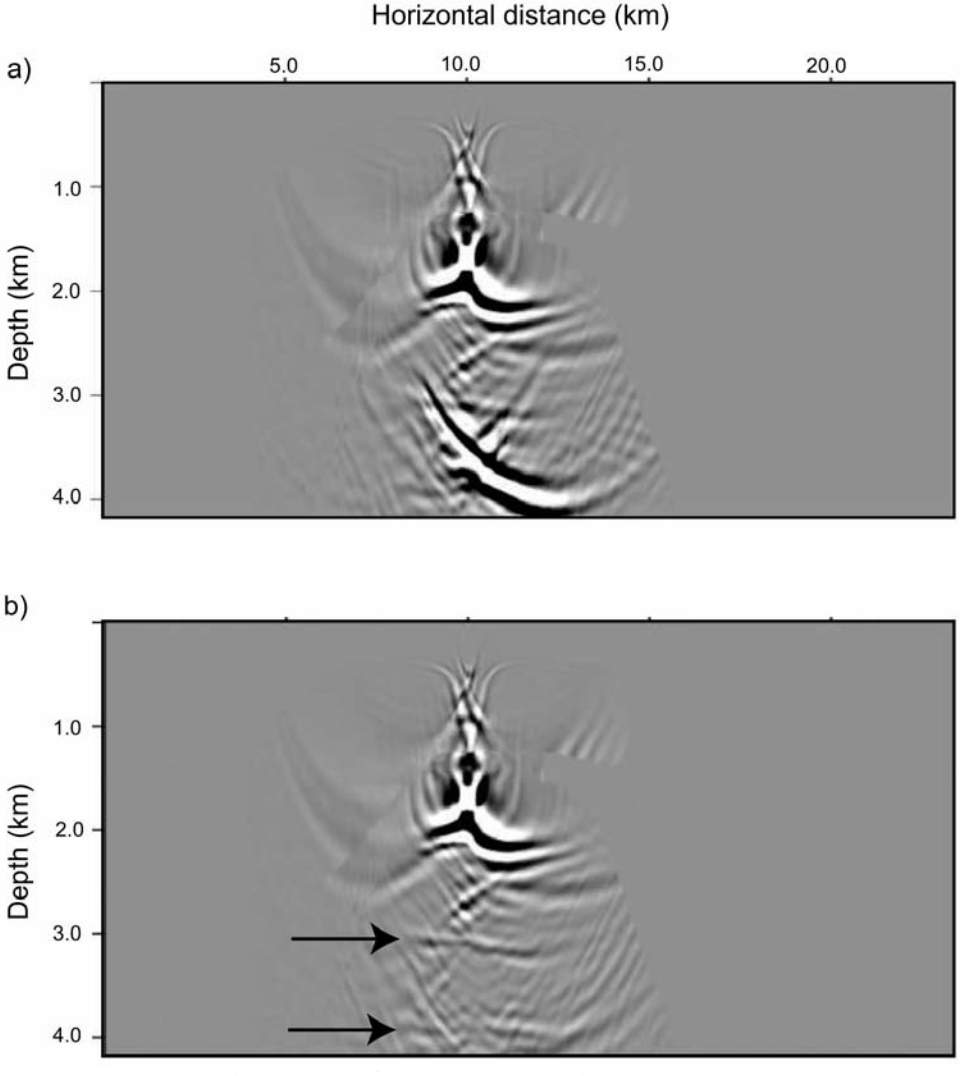

Fig. 8. Migration of a single CSG (a) before, and (b) after, multiple removal. Note the increased visibility of the subsalt reflections at the arrows in (b). This CSG is the one in the right column in Fig. 7. Compare with the migration of the whole line in Fig. 9.

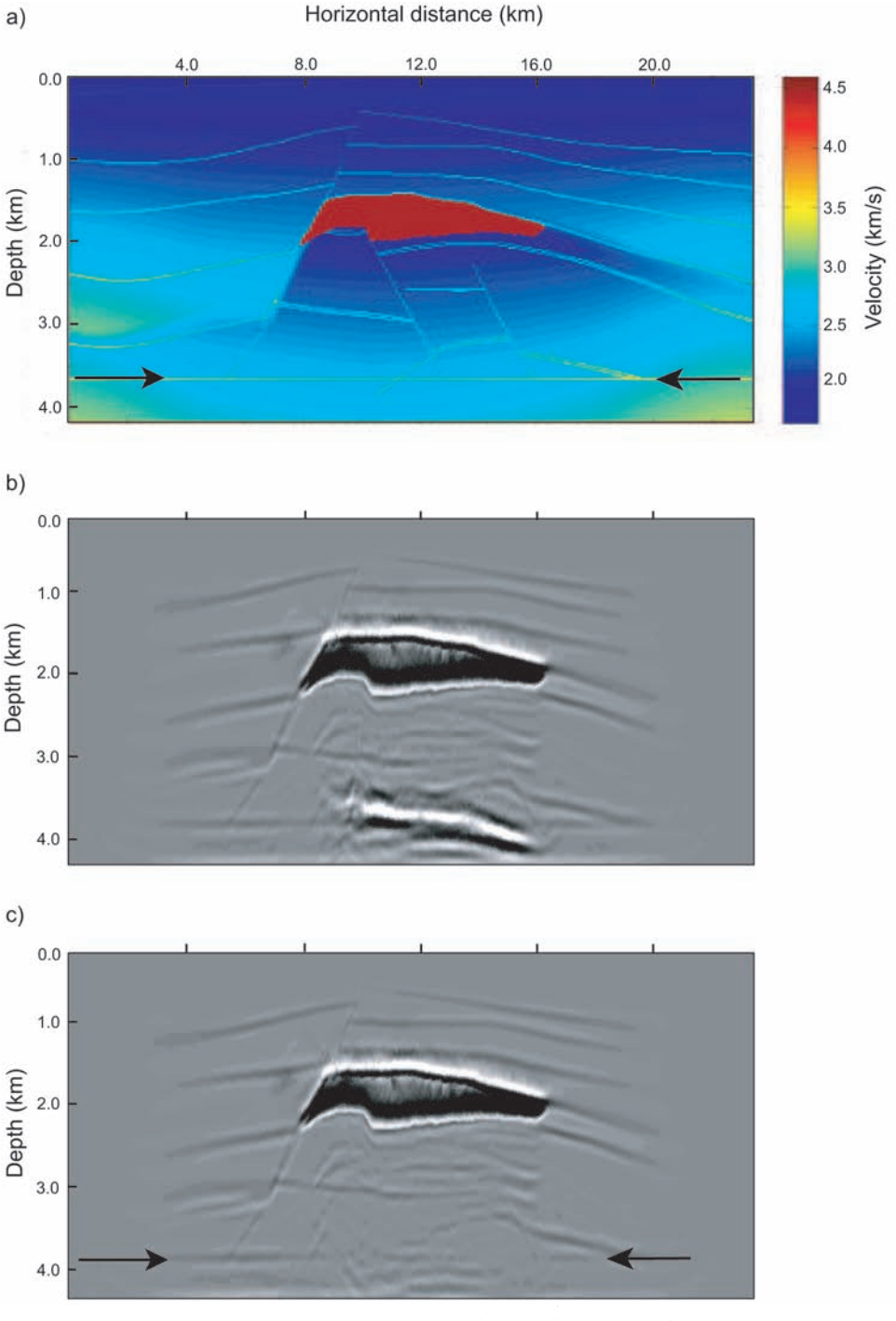

Fig. 9. Migrated sections. (a) velocity model used to generate the test data. (b) Migration without multiple removal. (c) Migration with multiple removal; compare (b) and (c) at the arrows.

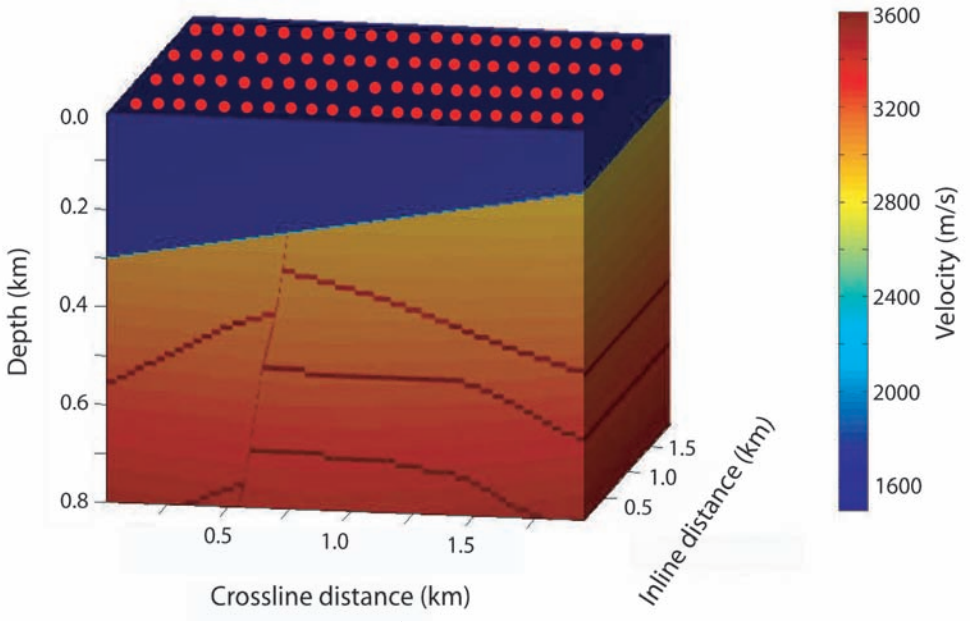

Fig.10. Velocity model used to generate 3D synthetic CSGs for free-surface multiple prediction and subtraction. The source inline and crossline intervals are 50 m; the receiver inline and crossline intervals are 5 m. The red dots on the upper surface represent every source in the crossline direction and evenly sampled sources in the inline direction.

Fig. 11 shows the x (inline) and y (crossline) components of slownesses for the water bottom reflection, computed from one CSG and one CRG. Fig. 12 shows the predictions of the first-and second-order multiples, of the water-bottom reflection, for a representative CSG. The predictions are plotted as the green curves on two crossline slices through the common-source volume (Fig. 13b); the predicted multiples overlie coherent events in the original data (Fig. 13a) well. The corresponding slices after multiple subtraction (Fig. 13c) show a significant reduction of the multiples, while retaining the primary reflections. As a comparison, Fig. 14 shows common-offset gathers estimated from a single representative 3D CSG with near, middle and far (100 m, 200 m, and 300 m) offsets before and after multiple subtraction.

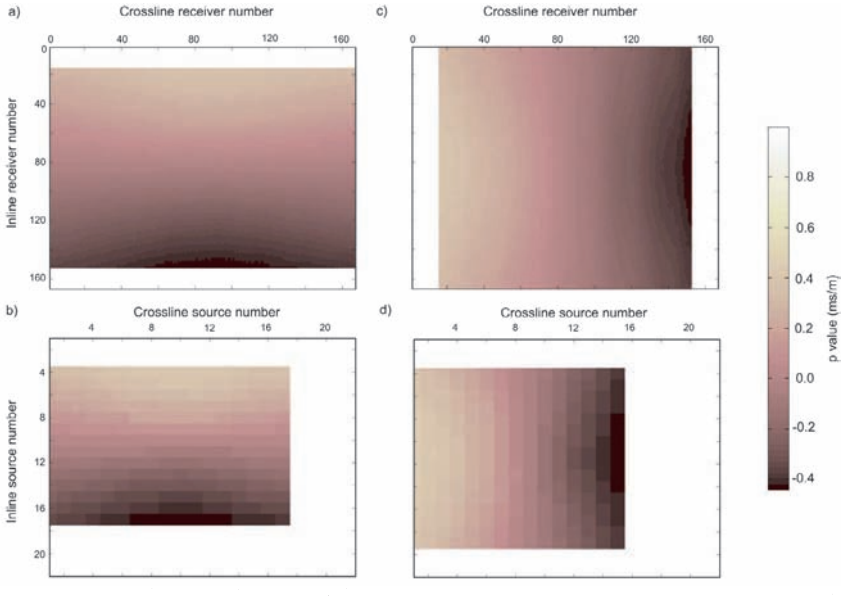

Fig. 11. (a) p_x-values in one CSG. (b) p_x-values in one CRG. (c) p_y-values in one CSG. (d) p_y-values in one CRG. These do not cover the complete 167 × 167 receiver array or the 22×22 source array because of the incomplete p-data recoverable at the edges of the centered p-value computation. The source for the CSG and the receiver for the CRG are both at inline 940 m and crossline 940 m.

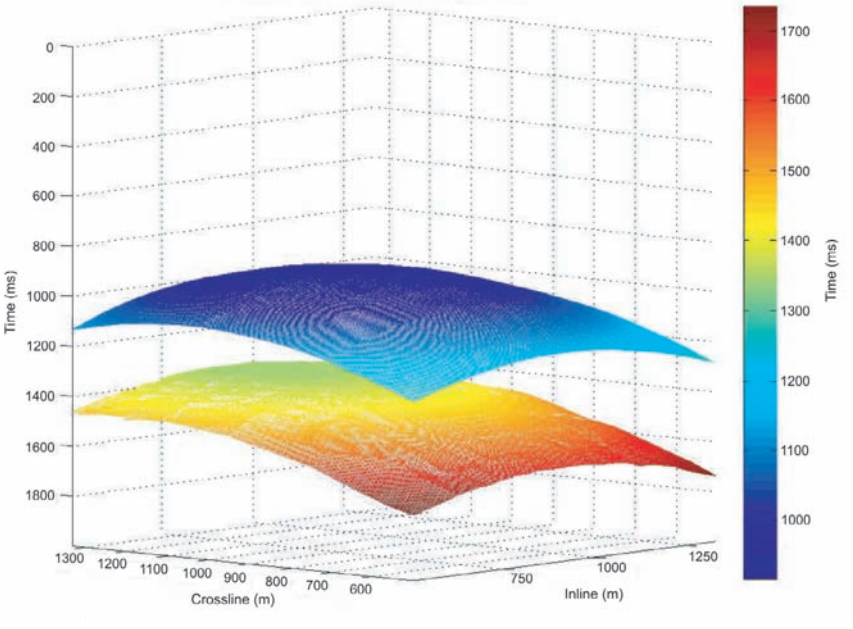

Fig. 12. The predictions of first and second free-surface to water-bottom multiples in a representative CSG. The source is located at inline 940 m and crossline 940 m in Fig. 10.

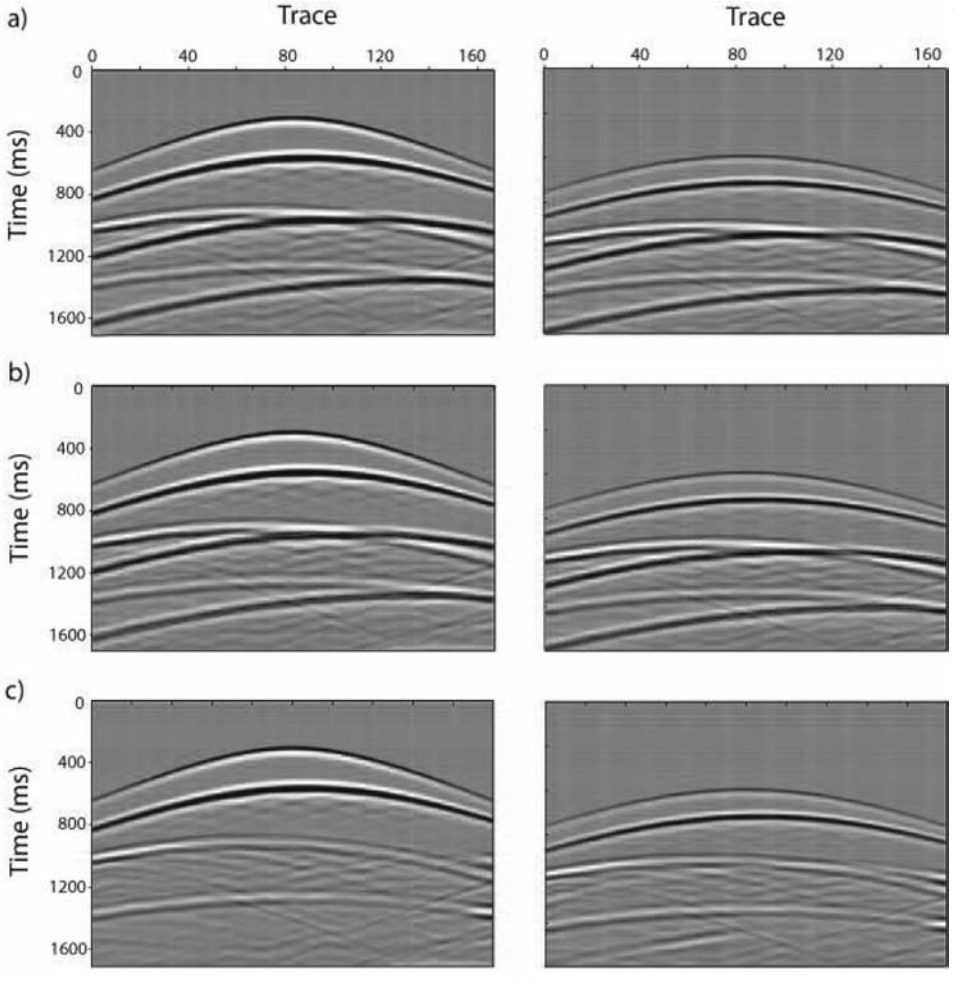

Fig. 13. Two input slices (a) of the same 3D CSG used in Fig. 11, with (b) predictions of free-surface multiples (superimposed in green), and (c) after multiple removal. These two (left and right) slices are located at inline locations 720 m and 1355 m, respectively, in the predicted surfaces in Fig. 12.

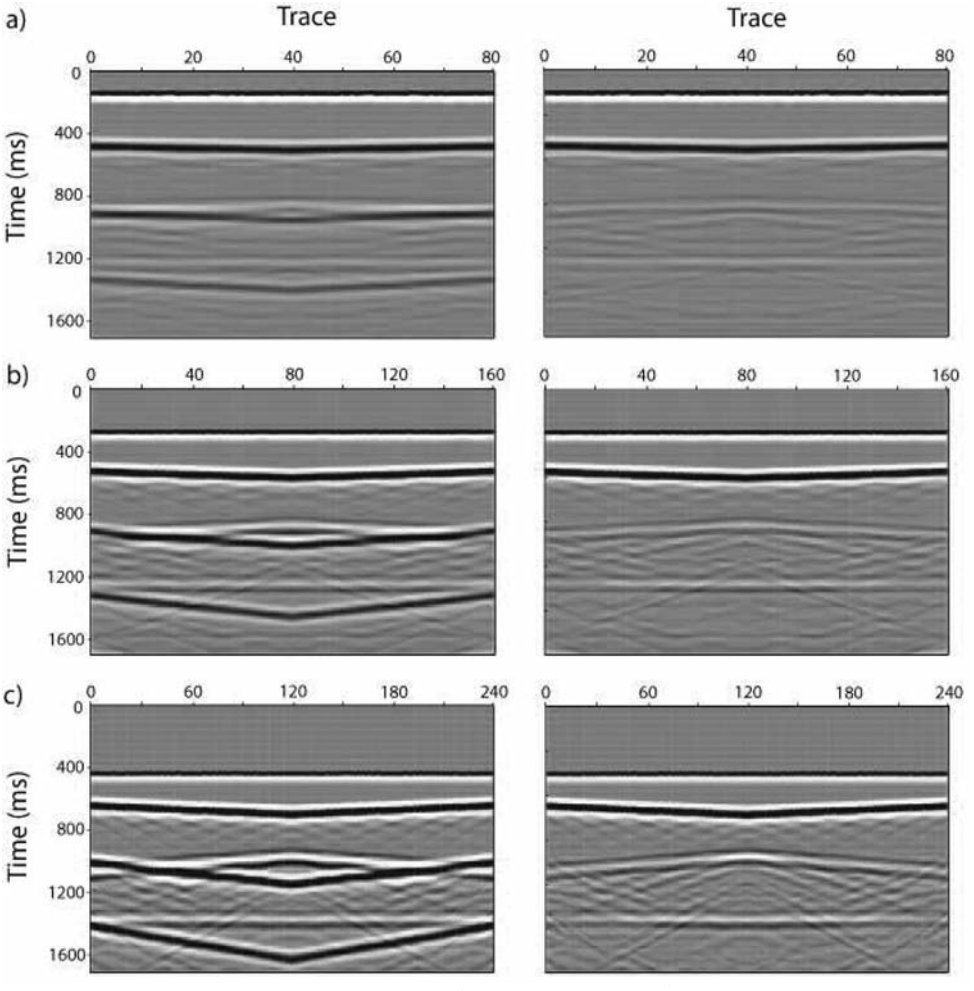

Fig. 14. The near offset (100 m) (a), middle offset (200 m) (b) and far offset (300 m) (c) sections before (left) and after (right) 3D multiple subtraction. These traces are on 3D (circular) receiver distributions centered on the source located at inline 940 m and crossline 940 m. The model is shown in Fig. 10.

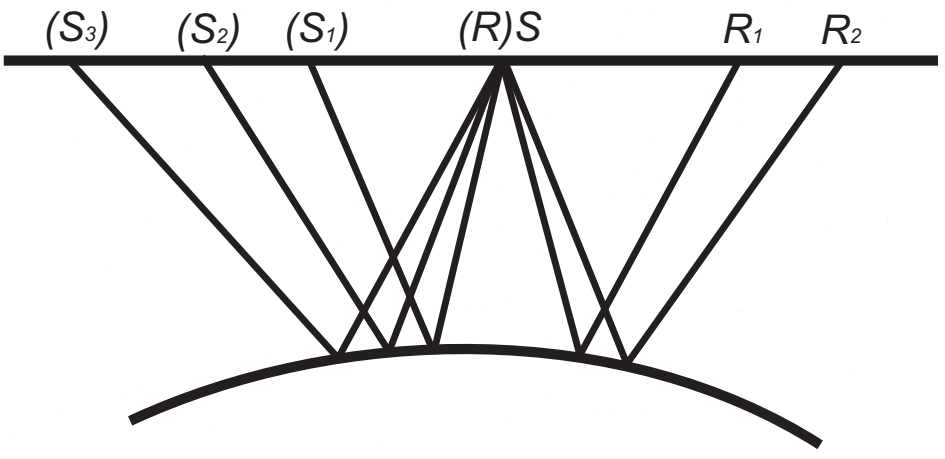

Fig. 15. Simulation of a split-spread data gather by combining a CSG (to the right) and a CRG (to the left), of off-end data, by setting the source and receiver locations S and R to coincide.

DISCUSSION

When primary and multiple reflections with similar apparent slownesses interfere with each other, multiple subtraction may damage the primaries if the local subtraction window is too small; residuals of the multiples may remain when the subtraction window is chosen to be too large. Determining time and trace windows with optimal bounds are important to achieve a good subtraction. If variations in velocity and subsurface structures are complicated, interference between primaries and multiples is localized, and will be compensated by the mixing that occurs during the subsequent migration.

This algorithm also works for data recorded on a land surface with variable topography because only apparent slownesses are calculated and matched. Accurate measurement of apparent p-values is the heart of the prediction procedure. The picked traveltimes may need to be smoothed to ensure stability in p-value matching in the prediction process.

As both $+p$ and $-p$ data need to be combined, only the sources away from the edges of a survey are surrounded by enough other sources to get continuous multiple predictions. In real 3D acquisition, the receiver apertures in the cross-line direction are often limited, so the main difficulty in the data preprocessing is to ensure sufficient source and receiver sampling for successful predictions. Wide aperture data, as in the examples above, are best.

In 3D data, when apparent horizontal slownesses are matched at each

reflection point, both x and y components need to be compared. Usually, p-values are not matched exactly and the nearest p is chosen when the exact one does not exist; this causes some prediction error. We interpolate the time predictions rather than p because the former is more efficient. To minimize the prediction error, picked traveltimes should be regularized and smoothed in areas where events interfere. Denser source and receiver sampling is simulated by interpolating traveltimes, which is equivalent to adding more sources between the original sources and increases accuracy when matching p-values.

A limitation of this algorithm is that picking of the primary reflections may be difficult for some datasets. For the main reflectors with large impedance contrasts, (e.g., a water bottom or a salt top) which generate the most important multiples, the primary picking is practical and straightforward to do automatically most of the time, with only a minimum of quality control needed.

Once the traveltimes of the primary reflections are picked from the CSGs, and the p-values are calculated from them, for all CSGs and CRGs, all the subsequent calculations for the multiple predictions are comparisons between different p-value matrices (not the field data volumes). Thus, computational efficiency is one of the strong advantages of this method. For example, the prediction and subtraction of multiples for a single source gather in the 2D example takes only seconds; even in the 3D example, it takes just 20 minutes for a single source gather using one workstation with two Intel(R) Core(TM) 2 processor CPUs, with a 2.40 GHz clock and 3.8 GB memory. A second major strength is that, to generate denser sampled sources and receivers to ensure accurate predictions, only traveltime interpolation is needed rather than trace interpolation. However, when data are sparse, or elevation changes rapidly through the data, interpolation may introduce new errors.

Sources of error also include time picking (which are magnified as successive multiples are predicted) and interpolation for local p-calculation. Time picking does not have to be excessively accurate; as long as the subtraction window encloses the multiple and follows it in shape. The more accurate the predicted shape, the better the removal. If there is substantial overlap between the predicted multiples and the primaries (in p-values, time and offset) the primary-multiple separation will not be complete. The effects of time-picking errors are not unique to this algorithm; they occur in most kinematic predictions of multiples from primaries (as listed in the Introduction).

The 2D split-spread field geometry provides the positive and negative slownesses required for prediction of multiples. However, a 2D split-spread gather can also be simulated by combining the CSG and CRG traces from an off-end survey geometry, by setting the source of the CSG and the receiver of the CRG at the same location (Fig. 15). This generalization is also applicable to 3D data.

CONCLUSIONS

The kinematic properties (traveltimes and offsets) of multiples are predicted from those of the primary reflections that produced the multiples. The selection of the primary reflections to concatenate is implemented through matching slownesses alternately at source and receiver positions. Only the arrival times of the primaries from the structures that produce multiples need to be identified and picked from the prestack CSG data to calculate the p-values for all CSGs and CRGs. The 2D procedure is extended to 3D by considering slowness as a three-component vector; in 3D, matching of apparent slownesses is between 3D vector components. Although the predictions involve no amplitude or phase information of the multiples, these are implicitly included in the data-adaptive, target-oriented subtraction; the wavelet to be subtracted from each trace is estimated locally by averaging across traces in a moving window. Wavelet estimation and subtraction are facilitated by flattening the multiple along its predicted time trajectory.

Results of the synthetic 2D and 3D data tests show that the algorithm works well, and without any knowledge or assumptions about the subsurface velocity or structure. The kinematic properties of free-surface multiples are successfully predicted using only the traveltimes and offsets of the primary reflections in the data. The subtraction effectively reduces the multiples in prestack data, with minimum damage to the primary reflections. The multiple removal is also easily observed in 2D and 3D depth migrated images and common offset gathers. After multiple subtraction, the primaries that were obscured beneath them are more coherent and geologically interpretable.

Our use of only the slownesses p in the multiple prediction eliminates many of the assumptions and complexities that are involved in previous algorithms; we do not need incident angles, velocities, radii of curvature, propagation paths, or the geometries of the free surface or of the reflectors. Unlike SRME, it does not do any wavefield convolutions, and so it is very cost effective.

ACKNOWLEDGMENTS

The research leading to this paper was supported by the sponsors of the UT-Dallas Geophysical Consortium and a UT-Dallas Geosciences teaching assistantship. The authors appreciate constructive comments provided by the reviewers. The time picking was done using WinPICS software provided by Divestco. This paper is Contribution No. 1218 from the Geosciences Department at the University of Texas at Dallas.

REFERENCES

Berkhout, A.J., 1982. Seismic Migration. Imaging of Acoustic Energy by Wave Field Extrapolation. Elsevier Science Publishing Company, Amsterdam.

Berkhout, A.J., 2006. Seismic processing in the inverse data space. Geophysics, 71: A29-A33.

Berkhout, A.J. and Verschuur, D.J., 1997. Estimation of multiple scattering by iterative inversion, Part 1: Theoretical considerations. Geophysics, 57: 1586-1595.

Berkhout, A.J. and Verschuur, D.J., 2007a. Seismic processing in the inverse data space, removal of surface-related and internal multiples. Extended Abstr., 69th EAGE Conf., London: B036.

Berkhout, A.J. and Verschuur, D.J., 2007b. Time-lapse processing in the inverse data space. Expanded Abstr., 79th Ann. Internat. SEG Mtg., San Antonio: 2919-2923.

Biersteker, J., 2001. MAGIC: Shell's surface multiple attenuation technique. Expanded Abstr., 71st Ann. Internat. SEG Mtg., San Antonio; 1301-1304.

Cao, J. and McMechan, G.A., 2010. Multiple prediction and subtraction from apparent slowness relations in 2D synthetic and field ocean-bottom cable data. Geophysics, 75, 6: V89-V99.

Gasparotto, A.F., Weglein, A.B., Carvalho, P.M. and Stolt, R.H., 1994. Inverse scattering series for multiple attenuation: Am example with surface and internal multiples. Expanded Abstr., 64th Ann. Internat. SEG Mtg., Los Angeles: 1039-1041.

Herrmann, F.J., Wang, D. and Verschuur, D.J., 2008. Adaptive curvelet-domain primary multiple separation. Geophysics, 73, 3: A17-A21.

Huo, S. and Wang, Y., 2009. Improving adaptive subtraction in seismic multiple attenuation. Geophysics, 74: V59-V67.

Kelamis, P.G., Zhu, W. and Rufaii, K.O., 2006. Land multiple attenuation -The future is bright. Expanded Abstr., 78th Ann. Internat. Mtg., New Orleans: 2699-2703.

Keydar, S., Landa, E., Gelchinsky, B. and Belfer, I., 1998. Multiple prediction using the homomorphic-imaging technique. Geophys. Prosp., 46: 423-440.

Landa, E., Belfer, I. and Keydar, S., 1999a. Multiple attenuation in the parabolic τ-p domain using wavefront characteristics of multiple-generating primaries. Geophysics, 64: 1806-1815.

Landa, E., Keydar, S. and Belfer, I., 1999b. Multiple prediction and attenuation using wavefront characteristics of multiple-generating primaries. The Leading Edge, 18: 6064.

Liu, F., Sen, M.K. and Stoffa, P.L., 2000. Dip selective 2-D multiple attenuation in the plane wave domain. Geophysics, 65: 264-274.

Ma, J., Sen, M.K. and Chen, X., 2009. Free-surface multiple attenuation using inverse data processing in the coupled plane-wave domain. Geophysics, 74: V75-V81.

Reshef, M., Arad, S. and Landa, E., 2006. 3D prediction of surface-related and interbed multiples. Geophysics, 71: V1-V6.

Van Dedem, E.J., 2002. 3D Surface-Related Multiple Prediction. Ph.D. thesis, Delft University of Technology.

Van Dedem, E.J. and Verschuur, D.J., 2005. 3D surface-related multiple prediction: A sparse inversion approach. Geophysics, 70: V31-V43.

Verschuur, D.J., 1991. Surface-related Multiple Elimination, an Inversion Approach. Ph.D. thesis, Delft University of Technology.

Verschuur, D.J., Berkhout, A.J. and Wapenaar, C.P.A., 1992. Adaptive surface-related multiple elimination. Geophysics, 57: 1166-1177.

Weglein, A.B., 1999. Multiple attenuation: An overview of recent advances and the road ahead. The Leading Edge, 18: 40-44.

Weglein, A.B. and Gasparotto, F.A., 1997. An inverse-scattering series method for attenuating multiples in seismic reflection data. Geophysics, 62: 1975-1989.

Zaske, J., 2000. Identification and Attenuation of Multiple Reflections Using Wavefront Characteristics. Ph.D. thesis, Karlsruhe University.